Effect of grain size on the recovery strain in a new Ti–20Zr–12Nb–2Sn superelastic alloy

J.-J. J Gao, I. Thibon, P. Castany, T. Gloriant

Effect of grain size on the recovery strain in a new Ti–20Zr–12Nb–2Sn superelastic alloy

J.-J. Gao, I. Thibon, P. Castany, T. Gloriant

Effect of grain size on the recovery strain in a new Ti-20Zr-12Nb-2Sn superelastic alloy

J.J. Gao, I. Thibon, P. Castany, T. Gloriant*

Univ Rennes, INSA Rennes, CNRS, ISCR UMR 6226, 35000 Rennes, France

*Corresponding author: e-mail: Thierry.Gloriant@insa-rennes.fr

Abstract:

In this study, the superelastic performance of a new β-type Ti-20Zr-12Nb-2Sn alloy has been investigated by means of cyclic tensile tests, electron back-scattered diffraction (EBSD) and in situ synchrotron X-ray diffraction (SXRD). It is shown that the β-grain size has an important influence on the superelastic property and for the same crystallographic texture, the smaller the grain size, the greater the recovery strain.

Keywords: titanium alloy; superelasticity; grain size; texture.

1. Introduction

NiTi alloys are widely used for the manufacture of various biomedical devices, such as orthodontic arches, orthopedic staples or endovascular stents thanks to their excellent superelastic property. However, their biocompatibility is an issue with such materials because of their high concentration of nickel, which can induce Ni-hypersensitivity and carcinogenic effect [1]. As the result, Ni-free metastable β titanium alloys are being developed as new superelastic alloys for biomedical applications. Thus, various titanium-based alloys elaborated from Ti-Nb-Al, Ti-Nb-Zr, Ti-Nb-Ta, Ti-Nb-Si, Ti-Nb-Zr-Sn, Ti-Nb-Zr-Ta or Ti-Nb-Ta-Zr-O systems [2-11] have shown superelastic properties due to the reversible stress-induced martensitic

transformation (SIM) occurring between the parent body-centered cubic β phase and the C-centered orthorhombic α" martensitic phase. However, the recovery strain remains fairly low with these alloys in comparison with NiTi. For instance, the measured recovery strain of superelastic Ti-Nb based alloys does not exceed 3% [12], which remains much lower than the value obtained with NiTi (around 8%). Therefore, improving the recovery strain of superelastic β-titanium alloys has become a major objective for metallurgists who carry out research on these alloys. In these alloys, the martensitic transformation temperature is greatly influenced by the β stabilizing elements. As for example, Kim et al. [2] showed that the martensitic transformation start temperature (M_s) decreases by 40K for a 1 at.% increase in the Nb content. These authors [13] also reported that the neutral alloying element Zr can increase significantly the transformation strain. Therefore, based on the superelastic Ti-27Nb alloy composition, the alloying element Nb was substituted by Zr and several new (Ti-Zr)-based alloy compositions were thus designed and characterized [14-15]. In the present work, a new superelastic Ti-20Zr-12Nb-2Sn alloy was optimized by choosing a suitable balance between Zr and Nb, and Sn was added to suppress the formation of ω phase [16] in order to improve further the superelastic recovery strain. More particularly, the effect of the β-grain size on its superelastic property was investigated by means of cyclic tensile tests, electron back-scattered diffraction (EBSD) and in situ synchrotron X-ray diffraction (SXRD).

2. Materials and methods

Raw metals (99.95% pure titanium, 99.078% pure zirconium, 99.9% pure niobium, 99.99% pure tin) were melted by the cold crucible levitation melting (CCLM) technique under argon atmosphere for the synthesis of the Ti-20Zr-12Nb-2Sn (at.%) alloy. The obtained ingot was homogenized at 950°C for 1200 min under high vacuum (10^{-7} mbar), followed by a water quenching. Then, the ingot was cold-rolled at room temperature until 95% reduction rate in thickness. Dog-bone tensile specimens were cut from the cold-rolled sheet into normalized

shape: 3 mm width, 0.5 mm in thickness and a gage length of 15 mm. In order to restore a fully recrystallized β microstructure from the cold-rolled state, the tensile specimens were finally heat-treated under high vacuum (10^{-7} mbar) with three different conditions in order to obtain different grain size distributions: a short thermal treatment (or flash treatment FT) at 560°C for 2 min (FT-560-02 specimens) and two solution treatments (ST) at 560°C and 700°C for 30 min (ST-560-30 and ST-700-30 specimens), respectively. The heat treatment temperatures were chosen above the beta-transus temperature, which was determined at 550°C by the electrical resistivity method [15] for the present Ti-20Zr-12Nb-2Sn alloy.

Tensile tests with the strain rate of 10^{-4} s^{-1} were performed to evaluate the mechanical properties of the different heat-treated samples. The tensile direction was chosen parallel to the cold rolling direction (RD). In this study, cyclic loading-unloading tensile tests were particularly employed in order to evaluate the recovery strain. For that, tensile stress is applied until the strain reaches 0.5% for the first cycle, and then the load is removed. The measurement is repeated through increasing the strain by 0.5% steps upon loading for the same specimen. An extensometer was used to measure the strain of the specimens during these tests.

To characterize the microstructure after the different heat-treatments, electron back-scattered diffraction (EBSD) analyses were conducted with a scanning electron microscope (Jeol JSM 7100F, SEM) equipped with an Oxford HKL EBSD system. Prior to the EBSD observations, all samples were mechanically mirror-polished by using several SiC papers with decreasing grid size and followed by colloidal silica suspension (particles size: 0.05 µm). In this work, the colloidal silica suspension was mixed with H_2O_2 solution to release stress due to polishing and reveal the microstructure.

In situ SXRD analyses under cyclic tensile tests were conducted in this study. SXRD experiments were carried out at the ID-22 high resolution powder diffraction beamline of the European Synchrotron Radiation Facility (ESRF, Grenoble, France) with 1.0×1.0 mm^2 X-ray beam size and a 0.35453630Å wavelength radiation. Diffractograms were acquired during in situ cyclic tensile test (at the rate of $10^{-4}s^{-1}$)

with strain increments of 0.5% until 3.5% of strain and then increased by 1.0% until 4.5% during each loading and unloading condition. Nine-channel detector was employed to collect transmitted diffracted beams from $2\theta=6°$ to $2\theta=20°$ for each cycle.

3. Results and discussion

Fig.1 shows the cyclic loading-unloading tensile curves from 0% to 5% of applied strain for the Ti-20Zr-12Nb-2Sn specimens heat-treated under the three conditions: (a) FT-560-02, (b) ST-560-30 and (c) ST-700-30, respectively. All engineering cyclic stress-strain curves confirm the superelastic behavior of these thermally treated alloys: a stress plateau is clearly visible, which is associated with the presence of hysteresis between loading and unloading curves due to the reversible SIM transformation between β and α" phases that occurs [12,15]. In the present study, the critical stress for slip, σ_{css}, is defined as the stress from which a residual plastic deformation starts to appear after unloading (the corresponding cycle is highlighted in bold on each curve). The different measured σ_{css} associated with their recovery strain values, ε_r, are indicated by dashed lines with arrows on the figures. As it is observed in Fig.1(a-c), the maximum recovery strain, ε_r=4.5%, and the highest critical stress for slip, σ_{css}=800 MPa, are obtained for the FT-560-02 specimen. Thus, it can be concluded that the superior superelastic property of the Ti-20Zr-12Nb-2Sn alloy for the short thermal treatment at 560°C for 2 min is directly due to its highest σ_{css} value.

In order to investigate the effect of the different heat-treatments on the superelastic recovery strain, the crystallographic orientation is investigated by EBSD for each sample. Fig.2 displays the inverse pole figure (IPF) maps obtained on FT-560-02 (a), ST-560-30 (b) and ST-700-30 (c) specimens along the cold rolling direction. The colors of the grains correspond to the different crystallographic orientations of the grains in the maps, as shown by the inserted color code for the rolling direction. Red, green and blue colors correspond then to $<001>_\beta$, $<101>_\beta$ and $<111>_\beta$ orientations, respectively, which are parallel to the cold-rolling direction. All

the samples show a typical equiaxed β-grain microstructure. As observed, a large majority of the grains are green indicating a strong $\{hkl\}_\beta<101>_\beta$ texture. Fig.2(d) presents the grain size distributions (≤10 μm) for the 3 samples and the averaged grain size is evaluated to be 0.4±0.3 μm, 1.6±1.1 μm and 7.3±4.8 μm for FT-560-02, ST-560-30 and ST-700-30, respectively. There are much more ultra-fined grains in the FT-560-02 alloy than in the two other ones. On the other hand, the ODFs (orientation distribution functions) have been calculated for each sample (available as supplementary materials) to furthermore verify the crystallographic orientation accurately and the corresponding IPFs are shown in Fig.3. In these IPFs, RD is the rolling direction and ND is the normal direction. The three IPFs from Fig.3(a) to Fig.3(c) confirm the same strong $\{111\}_\beta<101>_\beta$ recrystallization texture, which corresponds to a preferential orientation on the γ fiber as displayed in ODFs (supplementary material).

In this study, the martensitic transformation was characterized by SXRD under cyclic tensile tests. Fig.4(a) displays the initial SXRD pattern (in black) and the final SXRD patterns until 4.5% of applied strain (in red) and after unloading (in blue) for the FT-560-02 alloy. Prior to deformation, only the β phase and its typical diffraction peaks are observed: $(110)_\beta$, $(002)_\beta$, $(112)_\beta$, $(202)_\beta$, $(013)_\beta$. After being deformed to 4.5%, the mainly detected peaks correspond to SIM α" martensitic phase and they are indexed in Fig.4(a) for the loading condition. After unloading, β phase is again detected as the main phase and coexists with some residual SIM α" phase. The SIM transformation is thus clearly evidenced in the present Ti-20Zr-12Nb-2Sn alloy. In order to highlight the evolution of the stress-induced transformation, the evolution of the most intense β phase peak and SIM α" martensitic phase peaks is presented in Fig.4(b) within the restricted 7.6 - 9.4° angle range during the entire cyclic tensile test on loading and after unloading. It can be noticed that the $(110)_\beta$ peak shifts to the left on loading and returns back to its initial position after unloading. The $(002)_{\alpha"}$, $(020)_{\alpha"}$, $(021)_{\alpha"}$ martensitic peaks start to be detected from 1% of strain, which is in good agreement with the cyclic tensile curve. Up to 3.5% of strain, all α" peaks disappeared after unloading meaning that α" phase has transformed back into β phase

demonstrating thus a complete reversibility of the stress-induced martensitic transformation. However, a residual $(020)_{\alpha''}$ peak is still visible after unloading when the alloy was strained up to 4.5%. This observation corroborates the fact that the alloy has started to deform plastically from this strain rate and that the generated dislocations prevent a complete reversibility.

As widely reported, the $<101>_{\beta}$ type texture is favorable for obtaining the highest recovery strain [2,3,5], because the transformation strain is maximum between the parent body-centered cubic β phase and the C-centered orthorhombic α'' martensitic phase when loading along the $<101>_{\beta}$ direction. In our case, all the three heat-treated samples present the same $<101>_{\beta}$ type recrystallization orientation, but the corresponding recovery strains are very different, especially for the short treated sample for which the recovery strain is the highest one. It is well known that refined grains increase drastically the critical stress for slip, σ_{css}, in accordance with the classic Hall–Petch law [5,17-19]. The improvement of recovery strain is thus due to the high σ_{css} value (800 MPa) in the short treated sample (FT-560-02), which limits the formation of dislocations and, in turn, impedes the trapping of the martensitic phase by dislocations that allows a better reversibility of the stress-induced martensitic transformation. This result is consistent with previous works on (Ti-Nb)-based alloy [5,17,19-20]. On the contrary, in the case of the two ST samples containing larger grains, the stress-induced martensitic phase can be trapped by dislocations at a lower strain rate due to a lower critical stress for slip (585 MPa and 500 MPa for ST-560-30 and ST-700-30 respectively). Consequently, dislocations prevent the reversion of the orthorhombic lattice into the body-centered cubic lattice during unloading and thus the recovery strain becomes lower [20]. Therefore, this study shows that the grain size has an important influence on the superelastic property. It has thus been demonstrated for the same texture that the smaller the grain size, the greater the recoverable strain.

4. Conclusion

In this work, a new superelastic Ti-20Zr-12Nb-2Sn alloy was elaborated and investigated. After three different heat-treatments, it was observed by EBSD that the Ti-20Zr-12Nb-2Sn alloy presents the same strong $\{111\}_\beta<101>_\beta$ recrystallization texture but different average grain sizes. In situ SXRD investigations clearly revealed the reversible transformation that occurs between the β phase and the SIM α" phase during loading-unloading tensile test. After a short heat-treatment at 560°C for 2 min, a remarkable recovery strain of 4.5% was obtained due to a very refined grain size (0.4±0.3 μm).

Acknowledgments

J.J. Gao acknowledges the China Scholarship Council (CSC) for his Ph.D financial support (No. 2016-6329). The authors also acknowledge the SCANMAT platform of the University of Rennes for providing access to SEM facilities and the ESRF (Grenoble, France) for the SXRD facilities.

Reference

[1] R. Köster, D. Vieluf, M. Kiehn, M. Sommerauer, J. Kähler, S. Baldus, T. Meinertz, C.W. Hamm, Nickel and molybdenum contact allergies in patients with coronary in-stent restenosis, The Lancet 356 (2000) 1895–1897.

[2] H.Y. Kim, Y. Ikehara, J.I. Kim, H. Hosoda, S. Miyazaki, Martensitic transformation, shape memory effect and superelasticity of Ti-Nb binary alloys, Acta Mater. 54 (2006) 2419–2429.

[3] T. Inamura, Y. Fukui, H. Hosoda, K. Wakashima, S. Miyazaki, Relationship between texture and macroscopic transformation strain in severely cold-rolled Ti-Nb-Al superelastic alloy, Mater. Trans. 45 (2004) 1083–1089.

[4] H. Hosoda, Y. Kinoshita, Y. Fukui, T. Inamura, K. Wakashima, H.Y. Kim, S. Miyazaki, Effects of short time heat treatment on superelastic properties of a Ti-Nb-Al biomedical shape memory alloy, Mater. Sci. Eng. A438 (2006) 870–874.

[5] F. Sun, S. Nowak, T. Gloriant, P. Laheurte, A. Eberhardt, F. Prima, Influence of a short thermal treatment on the superelastic properties of a titanium-based alloy, Scripta Mater. 63 (2010) 1053–1056.

[6] J.I. Kim, H.Y. Kim, T. Inamura, H. Hosoda, S. Miyazaki, Shape memory characteristics of Ti-22Nb-(2-8)Zr (at.%) biomedical alloys, Mater. Sci. Eng. A403 (2005) 334–339.

[7] A. Ramalohary, P. Castany, P. Laheurte, F. Prima, T. Gloriant, Superelastic property induced by low-temperature heating of a shape memory Ti-24Nb-0.5Si biomedical alloy, Scripta Mater. 88 (2014) 25–28.

[8] Y.L. Hao, Z.B. Zhang, S.J. Li, R. Yang, Microstructure and mechanical behavior of a Ti-24Nb-4Zr-8Sn alloy processed by warm swaging and warm rolling, Acta Mater. 60 (2012) 2169–2177.

[9] Y.L. Hao, S.J. Li, S.Y. Sun, C.Y. Zheng, R. Yang, Elastic deformation behaviour of Ti-24Nb-4Zr-7.9 Sn for biomedical applications, Acta Biomater. 3 (2007) 277–286.

[10] M. Besse, P. Castany, T. Gloriant, Mechanisms of deformation in gum metal TNTZ-O and TNTZ titanium alloys: A comparative study on the oxygen influence, Acta Mater. 59 (2011) 5982–5988.

[11] E. Bertrand, T. Gloriant, D.M. Gordin, E. Vasilescu, P. Drob, C. Vasilescu, S.I. Drob, Synthesis and characterisation of a new superelastic Ti-25Ta-25Nb biomedical alloy, J.Mech. Behav. Biomed. Mater. 3 (2010) 559–564.

[12] P. Castany, Y. Yang, E. Bertrand, T. Gloriant, Reversion of a parent {130}<310>$_{\alpha''}$ martensitic twinning system at the origin of {332}<113>$_{\beta}$ twins observed in metastable β tanium alloys, Phys. Rev. Lett. 117 (2016) 245501.

[13] L.L. Pavón, H.Y. Kim, H. Hosoda, S. Miyazaki, Effect of Nb content and heat treatment temperature on superelastic properties of Ti-24Zr-(8-12)Nb–2Sn alloys, Scripta Mater. 95 (2015) 46–49.

[14] M.F. Ijaz, H.Y. Kim, H. Hosoda, S. Miyazaki, Superelastic properties of biomedical (Ti-Zr)-Mo-Sn alloys, Mater. Sci. Eng. C48 (2015) 11–20.

[15] J.J. Gao, I. Thibon, D. Laillé, P. Castany, T. Gloriant, Influence of texture and

transformation strain on the superelastic performance of a new Ti-20Zr-3Mo-3Sn alloy, Mater. Sci. Eng. A762 (2019) 138075.

[16] M.F. Ijaz, H.Y. Kim, H. Hosoda, S. Miyazaki, Effect of Sn addition on stress hysteresis and superelastic properties of a Ti-15Nb-3Mo alloy, Scripta Mater. 72 (2014) 29–32.

[17] Y. Al-Zain, H.Y. Kim, H. Hosoda, T.H. Nam, S. Miyazaki, Shape memory properties of Ti-Nb-Mo biomedical alloys, Acta Mater. 58 (2010) 4212–4223.

[18] M.F. Ijaz, D. Laillé, L. Héraud, D.-M. Gordin, P. Castany, T. Gloriant, Design of a novel superelastic Ti-23Hf-3Mo-4Sn biomedical alloy combining low modulus, high strength and large recovery strain, Mater. Lett. 177 (2016) 39–41.

[19] H.Y. Kim, S. Hashimoto, J.I. Kim, T. Inamura, H. Hosoda, S. Miyazaki, Effect of Ta addition on shape memory behavior of Ti-22Nb alloy, Mater. Sci. Eng. A417 (2006) 120–128.

[20] Y. Yang, P. Castany, M. Cornen, I. Thibon, F. Prima, T. Gloriant, Texture investigation of the superelastic Ti-24Nb-4Zr-8Sn alloy, J. All. Compds. 591 (2014) 85–90.

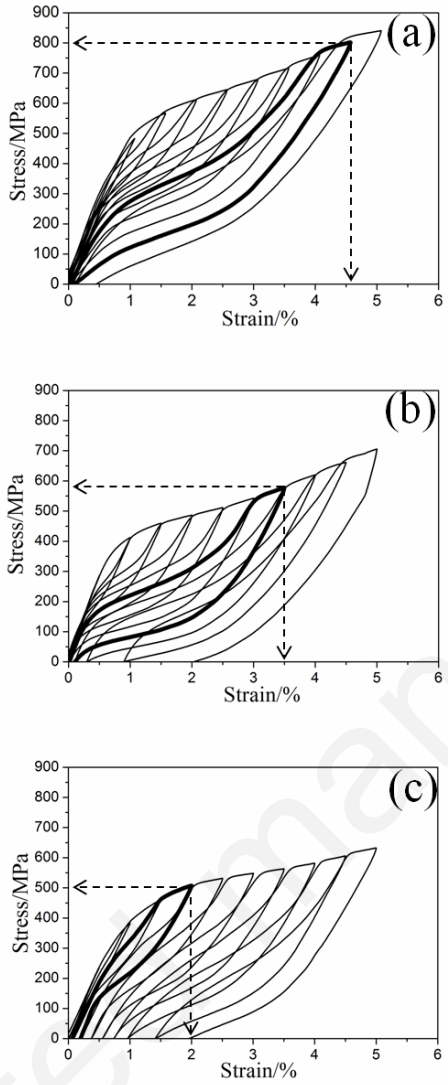

Fig.1 Engineering stress–strain curves of the first 5% strain obtained from cyclic loading–unloading tensile tests at room temperature for the heat-treated Ti-20Zr-12Nb-2Sn specimens: (a) FT-560-02; (b) ST-560-30; (c) ST-700-30.

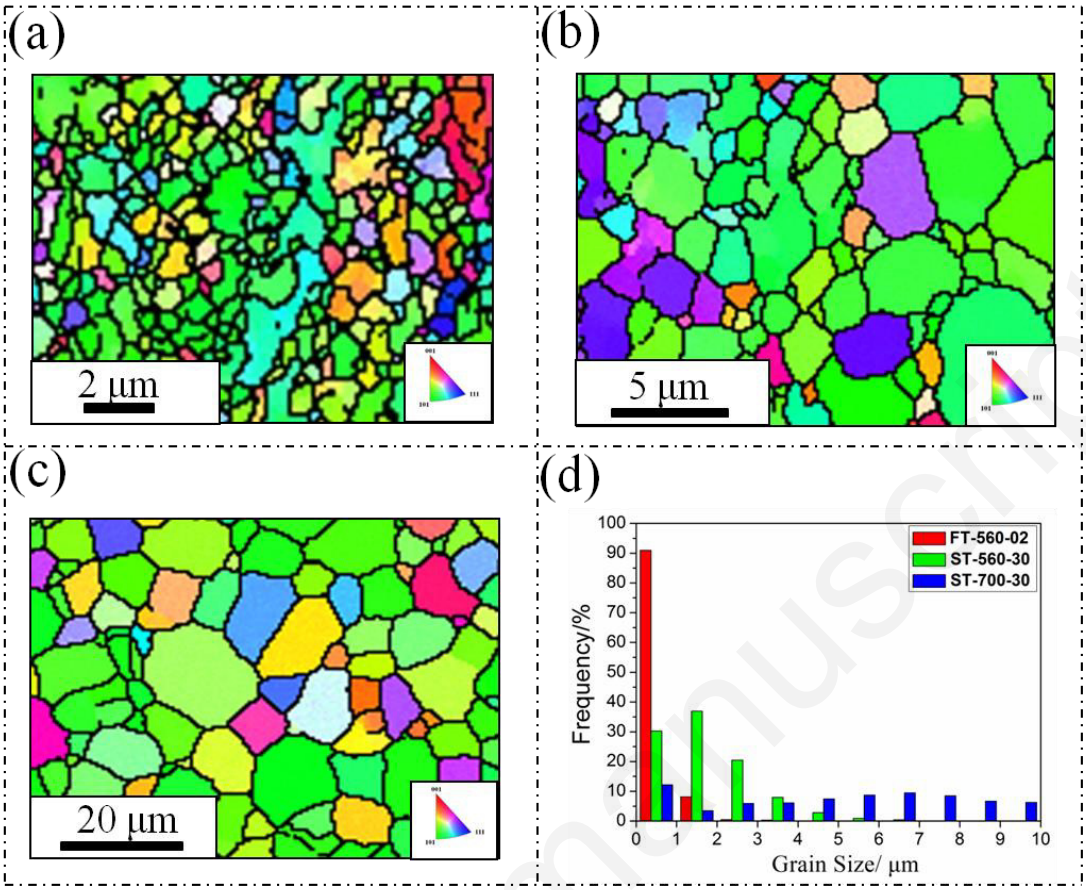

Fig.2 Inverse pole figure (IPF) maps along RD (Rolling Direction) for the heat-treated Ti-20Zr-12Nb-2Sn specimens: (a) FT-560-02; (b) ST-560-30; (c) ST-700-30; (d) the grain size (≤10 μm) distribution of the three heat treatment conditions.

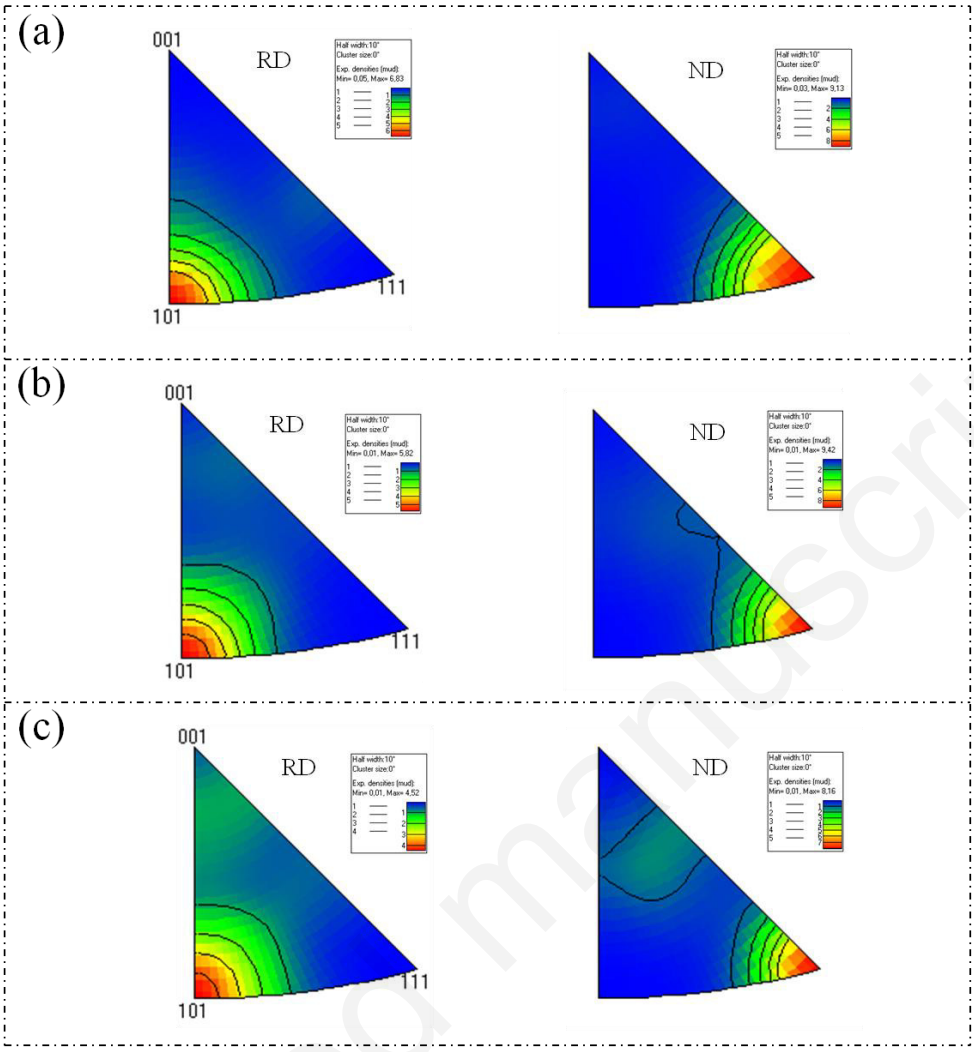

Fig.3 Inverse pole figures of the heat-treated Ti-20Zr-12Nb-2Sn specimens: (a) FT-560-02; (b) ST-560-30; (c) ST-700-30.

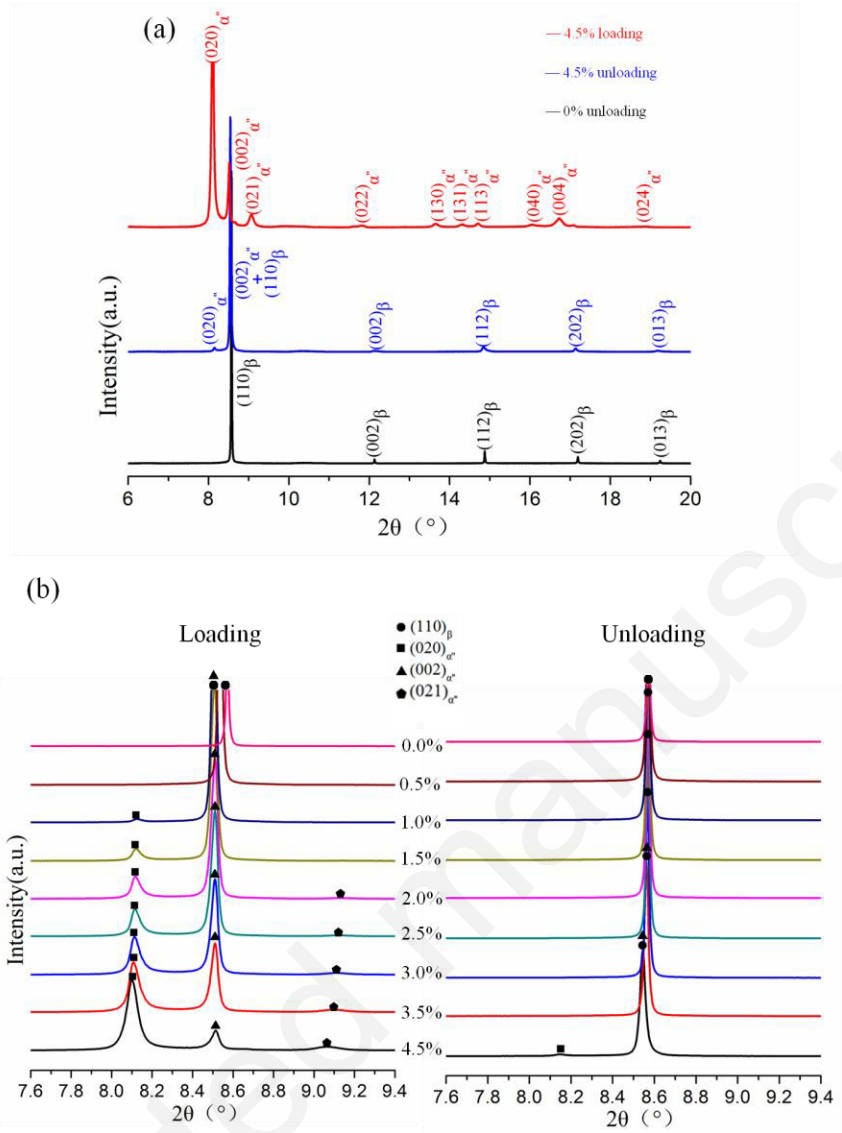

Fig.4 In situ SXRD patterns of the FT-560-02 alloy: (a) before deformation (black) and after 4.5% of strain during loading (red) and unloading (blue) conditions; (b) the zoomed patterns around 2θ=7.6°～9.4° during cyclic tensile tests on loading (left) and after unloading (right).